Title

Sulfur vacancy promoted peroxidase-like activity of magnetic greigite (Fe3S4) for colorimetric detection of serum glucose

Authors

Liu, Wei
Tian, Jinrong
Mao, Chengliang
et al.

Publication Date

2020-08-01

DOI

10.1016/j.aca.2020.06.056

Peer reviewed

Analytica Chimica Acta 1127 (2020) 246–255

Contents lists available at ScienceDirect

Analytica Chimica Acta

journal homepage: www.elsevier.com/locate/aca

Sulfur vacancy promoted peroxidase-like activity of magnetic greigite (Fe_3S_4) for colorimetric detection of serum glucose

Wei Liu [a, 1], Jinrong Tian [a, 1], Chengliang Mao [b], Zhenfeng Wang [a], Jia Liu [a], Randy A. Dahlgren [a], Lizhi Zhang [b], Xuedong Wang [a, c, *]

[a] Zhejiang Provincial Key Laboratory of Watershed Science and Health, College of Public Health and Management, Wenzhou Medical University, Wenzhou, 325035, People's Republic of China
[b] Key Laboratory of Pesticide & Chemical Biology of Ministry of Education, Institute of Environmental & Applied Chemistry, College of Chemistry, Central China Normal University, Wuhan, 430079, People's Republic of China
[c] National and Local Joint Engineering Laboratory of Municipal Sewage Resource Utilization Technology, School of Environmental Science and Engineering, Suzhou University of Science and Technology, Suzhou, 215009, People's Republic of China

HIGHLIGHTS

- SVs-rich Fe_3S_4 nanosheets are synthesized by adjusting ethylene glycol: water ratio.
- Sulfur vacancies promote the adsorption and decomposition of H_2O_2 on Fe_3S_4 surface.
- A colorimetric assay is constructed using SVs-rich Fe_3S_4 nanosheets, TMB and glucose.
- SVs-rich Fe_3S_4 nanosheets show higher peroxidase-like activity than SVs-poor Fe_3S_4.
- A smartphone APP is self-designed for the colorimetric detection of serum glucose.

GRAPHICAL ABSTRACT

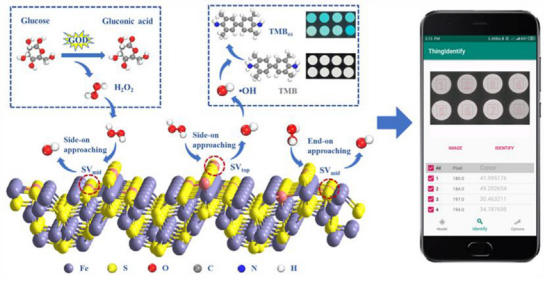

ARTICLE INFO

Article history:
Received 5 February 2020
Received in revised form
13 May 2020
Accepted 24 June 2020
Available online 10 July 2020

Keywords:
Fe_3S_4 nanosheets
S-vacancy
Peroxidase-like activity
Glucose detection

ABSTRACT

Herein, sulfur vacancies in magnetic greigite (SVs-Fe_3S_4) nanosheets were synthesized by a one-step solvothermal method by adjusting the ethylene glycol: water ratio. Electron paramagnetic resonance spectroscopy (EPR) and X-ray photoelectron spectroscopy (XPS) revealed that SV-rich Fe_3S_4 and SV-poor Fe_3S_4 were acquired using 100% ethylene glycol and 100% water as solvent, respectively. A peroxidase-like activity assay demonstrated that maximum reaction rates for H_2O_2-mediated oxidation of 3,3′,5,5′-tetramethyl-benzidine (TMB) catalyzed by the SV-rich Fe_3S_4 was 2.3 times higher than SV-poor Fe_3S_4. Density functional theory (DFT) calculations and reactive oxygen species (ROS) detection confirmed that the enhanced peroxidase-like activity by SV-rich Fe_3S_4 was attributed to efficient adsorption of H_2O_2 and subsequent decomposition to hydroxyl radicals (•OH) on the SVs sites of Fe_3S_4. The SV-rich Fe_3S_4 nanozyme was employed to develop a simple, highly sensitive and selective assay for glucose detection with a linear range of 0.5–150 μM and a detection limit of 0.1 μM (S/N = 3). A smartphone application (App) was designed and applied to efficiently detect serum glucose with the

* Corresponding author. Zhejiang Provincial Key Laboratory of Watershed Science and Health, College of Public Health and Management, Wenzhou Medical University, Wenzhou, 325035, People's Republic of China.
E-mail address: zjuwxd@163.com (X. Wang).
[1] Wei Liu and Jinrong Tian contributed equally to this work and share first authorship.

https://doi.org/10.1016/j.aca.2020.06.056
0003-2670/

Diabetes
Smartphone app

integrated analytical system based on the SV-rich Fe_3S_4. These new findings highlight the important role of surface defects in nanozymes on generating peroxidase-like activity for glucose detection in point-of-care diagnosis.

1. Introduction

As one of the most common diseases, diabetes is a chronic metabolic disease characterized by hyperglycemia and accompanied by a variety of complications associated with the heart, blood vessels, eyes, kidneys and nervous system [1,2]. The World Health Organization (WHO) reported that the global number of diabetes mellitus patients has risen to 422 million by 2015, and may increase to 693 million by 2045 [3]. Serum glucose, a major indicator of insulin-glucose dynamics in humans, plays a critical role in the evaluation of diabetes mellitus. Thus, early detection of elevated serum glucose concentrations has a profound impact on field analysis and point-of-care diagnosis applications.

To efficiently detect serum glucose in the laboratory, different methods including colorimetry [4], fluorometry [5], chemiluminescence [6], and electrochemistry [7] have been reported. Among these methods, colorimetric assays based on glucose oxidase-peroxidase (GOD-POD) are a widely used enzymatic method for serum glucose detection, owing to their rapid processing time, low detection limit, and high sensitivity. Briefly, glucose is first oxidized by oxygen in the presence of glucose oxidase to generate gluconic acid and hydrogen peroxide (H_2O_2). The H_2O_2 is then decomposed by catalase to form hydroxyl radicals (•OH), which oxidize 3,3′,5,5′-tetramethyl-benzidine (TMB) to 3,3′,5,5′-tetramethyl-benzidin (TMB_{ox}). The glucose concentration is a function of H_2O_2 and TMB_{ox} concentrations and can be calculated by measuring the colorimetric intensity of TMB_{ox} [8]. A disadvantage of this methodology is the use of natural catalase that is composed of proteins and RNA molecules rendering the assay relatively expensive with logistical issues related to difficult separation, environmental sensitivity, and specific storage requirements [9,10].

Nanomaterials, including metal oxide-based mimics [11,12], monometals/bimetallics [13,14], carbon-based nanostructures [15,16] and transition metal chalcogenides [17], are used as peroxidase-like nanozymes and employed to detect glucose based on colorimetric assays. For example, Hui and coworkers (2008) first developed an efficient H_2O_2-glucose analytical platform based on Fe_3O_4 nanoparticles, and found that the peroxidase-like activity of synthesized nano-Fe_3O_4 was higher than that of horseradish peroxidase (HRP) [10]. ESR spin-trapping techniques confirmed that the high peroxidase-like activities of $CoFe_2O_4$ resulted from the efficient decomposition of H_2O_2 into •OH via a Fenton-like reaction catalyzed by Fe(III) (Shi et al., 2011) [18]. Compared to natural enzymes, nanomaterial-based enzymes have attracted considerable attention for glucose detection owing to their low cost and ease of preparation, as well as their environmental stability and friendliness. The peroxidase-like activities of nanomaterial-based enzymes mainly depend on Fenton/Fenton-like reaction activity on the surface of nanomaterials [19,20]. Thus, increasing the Fenton/Fenton-like reactivity of nanomaterials plays a critical role in the accuracy and reliability of peroxidase-like nanozymes for practical applications.

Several surface structure constructions are employed to promote Fenton-like activity of nanomaterial surfaces for •OH generation. For example, Qu and co-workers (2019) successfully synthesized oxygen vacancies (OVs) in TiO_2 using a cyanide-assisted heat-treatment procedure, and demonstrated that the OVs promoted photocatalytic Fenton-like activity of Fe-based polyoxometalates/TiO_2. Electron spin resonance (ESR) confirmed that OVs on the TiO_2 favored electron transfer from TiO_2 to Fe-POM, resulting in enhanced production of $\bullet O^{2-}$ and •OH [21]. Li et al. (2017) developed a low-temperature, vacuum activated method to tune OVs concentrations on BiOCl, and demonstrated that the surface OVs acted as an electron-donor for H_2O_2 adsorption and dissociation to generate •OH via Fenton-like processes [22]. Liao and coworkers (2018) reported that the number of OVs in BiOBr could be regulated by changing the water/ethylene glycol ratio during the solvothermal process. The introduction of OVs provides abundant active sites and electrons for O_2 molecular adsorption and activation, which dramatically promotes the production of reactive oxygen species (ROS) for the photocatalytic removal of NO [23]. In sum, these studies conclude that the abundance of OVs on the catalyst surface was an important factor regulating H_2O_2 (O_2) adsorption and ROS generation via a heterogeneous Fenton-like reaction.

Owing to their specific effects on electron transfer processes, sulfur vacancies (SVs) on metal sulfides have gained attention for chemical and environmental applications. For example, Sun et al. (2019) found that SV-rich In_2S_3 nanosheets displayed excellent activity for selective photooxidation of alcohols to aldehydes compared to SV-poor In_2S_3 nanosheets, which resulted from enhanced electron transfer and O_2 activation with the introduction of surface SVs [24]. Moreover, as an electron-donating defect, sulfur vacancy in MoS_2 increased physical/chemical adsorption of O_2 and H_2O [25,26]. Recently, Xing et al. (2019) showed that unsaturated S atoms on the surface of metal sulfides capture protons from solution to form H_2S, and subsequently expose reductive metallic active sites to accelerate the rate-limiting Fe(III)/Fe(II) cycling in Fenton-like reactions for organic pollutant oxidation [27]. However, there is a paucity of information regarding the role of SVs in peroxidase-like activities of nanomaterial-based enzyme mimics in Fenton-like reactions.

Greigite (Fe_3S_4), an abundant iron sulfide mineral in sediments, is widely used for environmental applications. For example, Ding and co-workers (2016) investigated the peroxidase-like activity of Fe_3S_4 magnetic nanoparticles for glucose detection. They found that the pseudo-enzymatic activity of Fe_3S_4 was much higher than that of other magnetic nanomaterial-based enzymes [28]. Further, our previous study demonstrated that the structural S(−II) and Fe(II) of Fe_3S_4 are efficient reactive sites for Cr(VI), Fe(III), and organoarsenic redox transformations, and the reactivity of magnetic Fe_3S_4 depended on surface structural properties [29–32]. However, no data are currently available regarding the effects of Fe_3S_4 surface defects on peroxidase-like activity for colorimetric detection of glucose.

To address the research gaps identified above, this study constructed SV-rich and SV-poor Fe_3S_4 nanosheets, analyzed their differential peroxidase-like catalytic activities and utilized the SV-rich Fe_3S_4-based enzyme mimic for detection of glucose in serum samples. SV-rich and SV-poor Fe_3S_4 nanosheets were synthesized by modulating the solvent (EG/H_2O) mixing ratio. A series of conventional characterization techniques were used to identify surface

properties of the synthesized materials. Density functional theory (DFT) calculations were conducted to study H_2O_2 adsorption and decomposition on SVs of Fe_3S_4. The synthesized SV-rich Fe_3S_4 was used as a peroxidase-like nanozyme for serum glucose detection. The effects of SV concentration, incubation temperature, solution pH, and Fe_3S_4 dosage on the peroxidase-like activity of Fe_3S_4 were systematically investigated to optimize operational parameters. Finally, a smartphone application was designed and employed for fast detection of serum glucose in point-of-care diagnosis (Scheme 1).

2. Experimental

2.1. Materials and reagents

Acetic acid (CH_3COOH), sodium acetate (CH_3COONa), hydrogen peroxide (H_2O_2, 30%), ethanol, ethylene glycol (EG), L-cysteine, dimethyl sulfoxide (DMSO), ferrous sulfate ($FeSO_4•7H_2O$), glucose, maltose, lactose, and fructose were purchased from Sinopharm Chemical Reagent (Shanghai, China). Terephthalic acid (TA), 3,3′, 5,5′-tetramethyl benzidine (TMB), and glucose oxidase (GOD) were obtained from Aladdin Reagent (Shanghai, China). All chemicals were analytical grade and used as received without further purification. Deionized water was prepared by a Millipore Milli-Q system (Bedford, MA, USA) and used for all experiments. Serum samples were collected at the first affiliated hospital of Wenzhou Medical University (Wenzhou, China) following procedures approved by the Wenzhou Medical University Ethics Committee.

2.2. Synthesis of SV-based Fe_3S_4 nanosheets

The Fe_3S_4 nanosheets with varying degrees of SVs were synthesized using a one-step solvothermal method [33]. Briefly, homogenous solution A and B were prepared by dissolving 0.834 g $FeSO_4•7H_2O$ and 0.363 g L-cysteine in 30 mL of EG, respectively. Solution A was added dropwise to solution B within 2 min and magnetically stirred at ambient conditions for 20 min to form a colorless mixture. The mixture was subsequently transferred into a 100 mL Teflon-lined autoclave and heated at 180 °C for 12 h. After cooling to room temperature, the resulting solid product was separated using a magnet and sequentially washed three times with deionized water and ethanol before drying in a vacuum oven at 60 °C for 6 h. The final product was designated as FS-100 (i.e., 100% EG). To prepare Fe_3S_4 with varying degrees of SVs, the EG: H_2O ratio of the mixed solvent (60 mL total volume containing 30, 15 and 0 mL EG) was altered to acquire products referred to as FS-50, FS-25 and FS-0, respectively.

2.3. Characterization

Powder X-ray diffraction (XRD) patterns of the Fe_3S_4 nanosheets were obtained using a Bruker D8 Advance X-ray diffractometer (Bruker, Billerica, MA, USA) with Cu Kα radiation (λ = 0.15418 nm). Fe_3S_4 morphology and structure were characterized by scanning electron microscopy (SEM, Zeiss Sigma 300, Oberkochen, Germany) and high-angle annular dark field-scanning TEM (JEOL-JEM2010, Tokyo, Japan). Brunauer-Emmett-Teller (BET) surface area was computed using nitrogen adsorption/desorption isotherms with a nitrogen-adsorption system (Micromeritics Instruments Corp, Norcross, GA, USA). Electron paramagnetic resonance (EPR) spectroscopy was carried out on a Bruker EMX X-band spectrometer. Fe_3S_4 (20 mg) was put into a sealed quartz tube, which was then inserted into the EPR cavity, and the spectra were recorded at selected intervals. The microwave power, modulation frequency, and amplitude of EPR spectrometer were Ca 10.8 mW, 9.853 GHz, and up to 5 G, respectively. X-ray photoelectron spectroscopy (XPS) was measured on a Thermo ESCALAB 250Xi (Thermo Fisher Scientific, Waltham, MA, USA) with a monochromatic Al *Kα* source. All XPS peaks were calibrated using C1s (284.8 eV) as the reference. Zeta potentials for Fe_3S_4 suspensions at different pH values were determined by a Malvern ZEN3690 Zetasizer (Malvern, UK). Tafel curves were determined with a CHI−650C electrochemical workstation (CH Instruments, Austin, TX, USA).

2.4. DFT theoretical calculations

DFT calculations were performed using the *CASTEP* software package. The generalized gradient approximation (GGA) with Perdew-Burke-Ernzerhof (PBE) function was employed for the exchange-correlation function. During geometry optimization, all atoms were fully relaxed with an energy convergence of 5.0×10^{-5} eV/atom and a force convergence of 0.1 eV/Å, and the cutoff energy was set at 260 eV. The Monkhorst-Pack mesh for the Fe_3S_4 (011) surface was 1 × 1 × 1. To evaluate H_2O_2 adsorption and decomposition on the surface of Fe_3S_4, a 1 × 1 (011) surface with five atom layers was constructed. Then, the fate of molecular H_2O_2 was assessed as it approached the Fe_3S_4 surface with end-on or side-on adsorption. The adsorption energies of adsorbates were defined as:

$$E_{ad}(m) = E_{m\text{-}s} - E_s - E_m$$

where *m* represents adsorbate and *s* represents the surface of Fe_3S_4 (011).

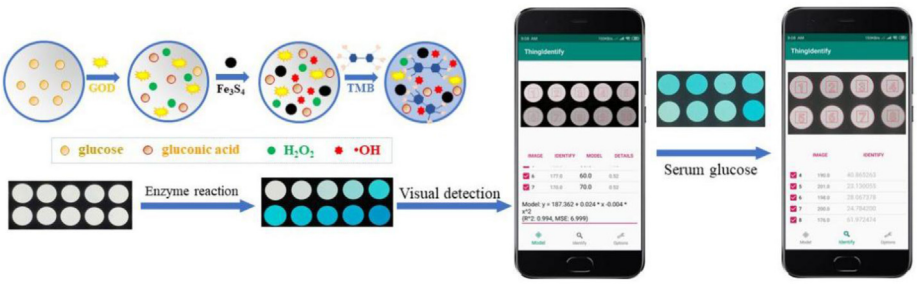

Scheme 1. Schematic of colorimetric probe and visual detection principle for glucose.

Scheme 1. Schematic of colorimetric probe and visual detection principle for glucose.

2.5. Peroxidase-like activity of SV-based Fe_3S_4

Peroxidase-like activities of Fe_3S_4 with varying degrees of SVs were evaluated by catalyzing the oxidation of TMB in the presence of H_2O_2. Steady-state kinetic experiments were carried out by adding various concentrations of H_2O_2 (0.01–0.80 mM) or TMB (0.1–1.6 mM) under optimized experimental conditions. Briefly, 60 μL of 1 mg/mL Fe_3S_4 suspension was added into 1700 μL NaAc-HAc buffer solution (20 mM, pH = 4.0) to form a mixture. Then, 200 μL of 6 mM TMB and 40 μL of 50 mM H_2O_2 were sequentially added to the above mixture. The suspension was incubated at 40 °C for 20 min forming a blue colored solution. The supernatant was decanted following sedimentation of the magnetic Fe_3S_4 with a magnet placed externally at the bottom of the reaction tube, and the supernatant was utilized for spectral measurement with a Shimadzu UV-2600 spectrophotometer (Kyoto, Japan) at a wavelength of 652 nm. Finally, the enzymatic parameters, V_{max} (maximal reaction rate) and K_m (Michaelis-Menten constant) were determined from Lineweaver-Burk plots.

2.6. Detection of •OH and ferrous iron concentrations

Terephthalic acid was used as a probe for detection of •OH [12]. A 2.0 mL aliquot of NaAc-HAc buffer solution (pH = 4.0) containing 50 mM H_2O_2 and 6 mM TA was incubated with 60 μL of 1 mg/mL Fe_3S_4 for 5, 10, 15 or 20 min. The reacted solution was separated using a magnet to remove the remaining magnetic Fe_3S_4. Fluorescence intensity of the generated 2-OH-terephthalic acid was recorded at 426 nm after excitation at 315 nm with a FS5 fluorescence spectrometer (Edinburgh Instrument, Livingston, UK). Dissolved Fe(II) concentration was quantified using 1,10-phenanthroline with detection by UV–Vis spectrometry at 510 nm [34].

2.7. Colorimetric detection of glucose

To acquire the glucose calibration curve, 100 μL glucose (0.5–150 μM) and 50 μL GOD (2 mg/mL) were mixed in 100 μL NaAc-HAc buffer solution (20 mM, pH = 7) before incubation at 37 °C for 30 min. The reacted solution was added to a mixture containing 200 μL TMB (6 mM), 60 μL Fe_3S_4 (1 mg/mL) and 1490 μL NaAc-HAc buffer solution (20 mM, pH = 4). After incubation at 40 °C for 20 min, the supernatant was decanted for spectral analysis after magnetic separation of the Fe_3S_4 solids.

Blood serum samples for glucose quantification were stored at −80 °C prior to pretreatment. Before analysis, the frozen samples were thawed at 4 °C and then centrifuged at 10,000 rpm for 20 min to remove any large aggregates. The supernatant was diluted 150 times with NaAc-HAc buffer (20 mM, pH = 7.0) to obtain the final serum samples. A 100 μL aliquot of serum and 50 μL GOD (2 mg/mL) were mixed in 100 μL NaAc-HAc buffer solution (20 mM, pH = 7) before incubation at 40 °C for 30 min. The reacted serum solution was added to a mixture containing 200 μL TMB (6 mM), 60 μL Fe_3S_4 (1 mg/mL) and 1490 μL NaAc-HAc buffer solution (20 mM, pH = 4). After incubation at 40 °C for 20 min, the supernatant was decanted for spectral analysis after magnetic separation of the Fe_3S_4 solids. Final serum glucose concentrations were calculated from the glucose calibration curve.

2.8. Smartphone application for glucose detection

The detection of glucose was conducted using an automated smartphone application (App). The smartphone colorimetry platform and the schematic illustration of the App procedures are shown in Schemes S1 and S2 and described in detail in Supporting Information.

3. Results and discussion

3.1. Fe_3S_4 nanosheet characterization

The crystalline phase and purity of as-synthesized Fe_3S_4 nanosheets were examined by XRD. Five specific diffraction peaks at 25.4°, 30.0°, 36.3°, 47.8° and 52.4° (Fig. 1A) were identified as the (220), (311), (400), (511) and (440) crystal planes of cubic Fe_3S_4 (JCPDS Powder Diffraction File No. 16–713). No impurities were detected in the XRD patterns, indicating high purity of the as-synthesized Fe_3S_4 nanosheets. Moreover, there was no difference between the four samples obtained using variable EG: H_2O ratios in the solvent, suggesting a limited effect of solvent on the crystalline phase.

SEM was employed to investigate the effects of EG: H_2O ratios on the size and shape of Fe_3S_4 products. All samples exhibited flower-like structure consisting of multiple nanosheets (Fig. S1). However, the “flower” size decreased from ~10 to ~4 μm with increasing EG concentrations from 0 to 100%, which may be ascribed to differences in the dielectric constant, interionic attraction and solute-solvent interactions on crystal growth formation [33]. TEM images revealed that high ratios of EG in the solvent resulted in the bending of nanosheets, consistent with SEM images. HR-TEM images of FS-0 (Fig. 1B) indicated a lattice spacing of 0.28 nm that was assigned to the (220) facet, which is perpendicular to the (011) facet. In contrast, the distinct lattice spacing for FS-100 was 0.58 nm, corresponding to the (440) facet that was perpendicular to the (011) facet (Fig. 1B). Thus, it can be concluded that both FS-0 and FS-100 exhibited (011) exposed facets (Fig. S2).

Presence of ethylene glycol in the reaction solvent is purported to induce formation of defects in the crystalline products [35]. Herein, the as-prepared Fe_3S_4 was examined by room-temperature EPR to detect SVs in the Fe_3S_4 nanosheets (Fig. 1C). A prominent signal with a spectroscopic splitting factor of 2.005 was observed for the as-prepared Fe_3S_4, confirming differences in SVs of Fe_3S_4 as a function of the EG: H_2O ratio of the solvent [24]. In particular, the EPR signal intensity of FS-100 (40010 a.u.) was much higher than FS-0 (7773.9 a.u.), suggesting that SVs in the Fe_3S_4 nanosheets were highly dependent on the EG: H_2O ratio. As a result, the SV-rich Fe_3S_4 (FS-100) and SV-poor Fe_3S_4 (FS-0) were obtained using 100% EG and 100% H_2O as solvents, respectively.

As SVs strongly influence the surface reactivity and elemental/structural composition of materials, XPS was utilized to verify the existence of SVs. High resolution XPS spectra of S 2p displayed three peaks at 161.3, 162.6 and 163.8 eV for FS-0 that were assigned to $S(-II)_{surface}$, $S(-II)_{bulk}$ and $S_n(-II)$, respectively (Fig. 1D) [36]. However, the specific peak location gradually shifted to lower binding energy for FS-25 (161.2 eV), FS-50 (161.1 eV) and FS-100 (160.9 eV), confirming the breakage Fe–S linkages resulting from an increasing abundance of SVs. Correspondingly, the high resolution spectra of Fe 2p exhibited four peaks at 707.1, 708.4, 710.5 and 711.5 eV for FS-0, which were attributed to $Fe(II)_{lattice}$, $Fe(II)_{surf}$ and $Fe(III)_{surf}$, respectively (Fig. S3B) [34]. Similar to the S 2p spectra, the specific peak locations for iron species gradually shifted to lower binding energy for FS-25, FS-50 and FS-100. Furthermore, the relative fraction of $Fe(II)_{surf}$ increased from 13.9% (FS-0) to 22.2% (FS-100) with a corresponding decrease in $Fe(II)_{lattice}$ from 16.6% (FS-0) to 7.2% (FS-100) (Table S1). Taken in total, these results confirm that SV concentrations on Fe_3S_4 can be easily tuned by adjusting the EG: H_2O ratio of the solvent used in the synthesis process; SV-rich Fe_3S_4 (FS-100) was successfully prepared using pure EG as the solvent.

Given that defect features in crystalline structures may strongly affect electron transfer properties, Tafel polarization diagrams were determined in NaAc-HAc buffer to assess electron diffusion rates in

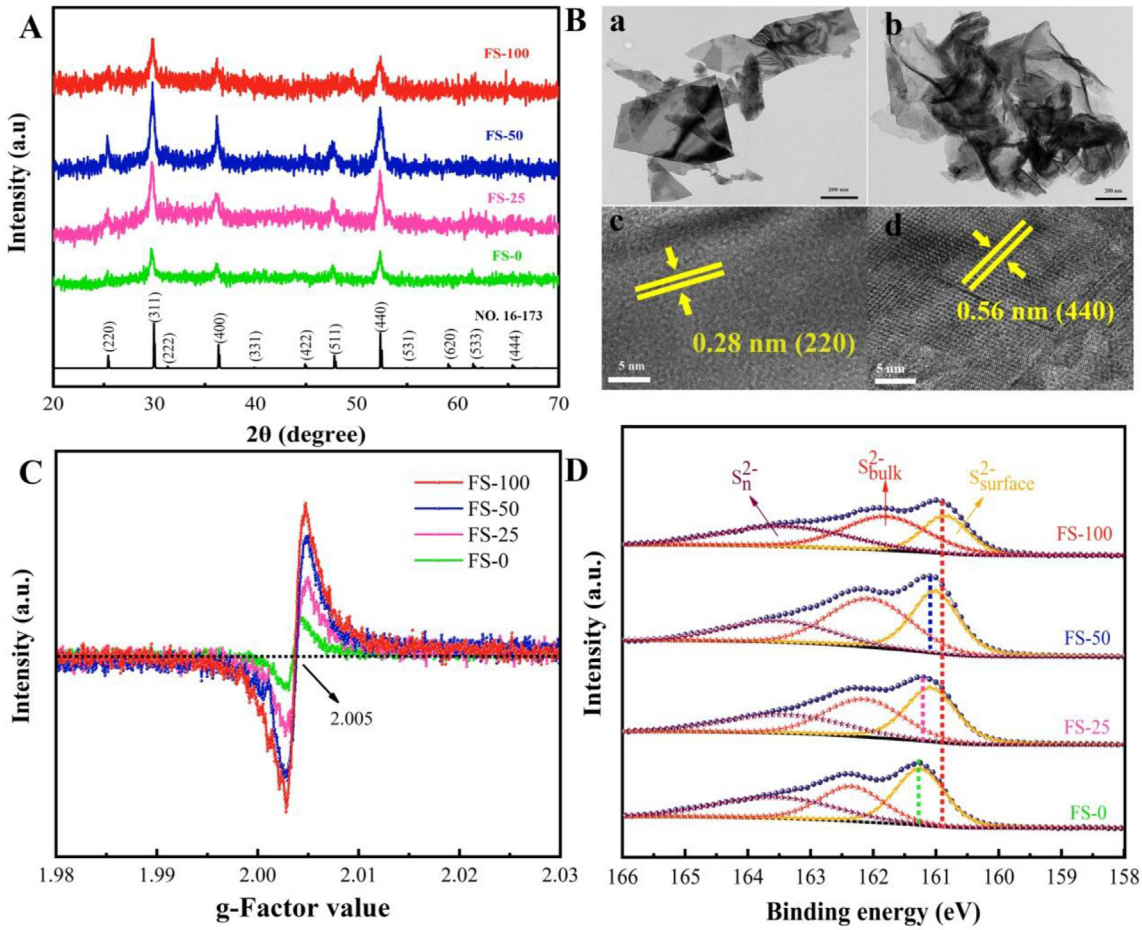

Fig. 1. (A) XRD patterns of as-prepared Fe_3S_4. (B) HRTEM images of FS-0 (a, c) and FS-100 (b, d). (C) Room-temperature EPR spectra and (D) S 2p XPS spectra of Fe_3S_4 nanosheets.

SV-based Fe_3S_4. Free corrosion potentials for SV-based Fe_3S_4 ranged from −0.05 to −0.11 V, and their negative potentials followed: FS-100 > FS-50 > FS-25 > FS-0 (Fig. S4). The negative free corrosion potentials were ascribed to higher electron transfer rates and suggest that higher SV concentrations on Fe_3S_4 promote electronic transfer processes.

To further study the effects of solvent ratios during the solvothermal synthesis process on the surface properties of Fe_3S_4 nanosheets, BET surface area and the surface potential were characterized. BET surface areas for Fe_3S_4 synthesized with 100% EG (FS-100, 20.0 m^2/g) and 100% H_2O (FS-0, 17.7 m^2/g) were higher than those with mixed solvents (FS-25 and FS-50; Table S2). Rownaghi et al. (2009) observed that the surface area of catalyst prepared by ethylene glycol was prominently larger than for catalyst prepared using water.[37] Zeta potential analysis showed that all SV-based Fe_3S_4 nanosheets had isoelectric points near pH 4.0, and the surface charge of FS-100 was more positive than FS-0 in neutral solutions (Fig. S5).

3.2. DFT theoretical calculations

To understand the role of SVs in Fe_3S_4 nanosheets for generating peroxidase-like activity leading to H_2O_2 decomposition, theoretical DFT calculations were investigated. Molecular H_2O_2 was first set to approach SVs on the Fe_3S_4 (011) surface for geometry optimization, and then the activation of H_2O_2 by SVs was quantitatively analyzed via stable adsorption configuration and adsorption energy. Since Fe atoms located in octahedral sites of the (011) surface, two types of surface exposed S atoms existed, namely top and middle sites on the (011) facet of the Fe_3S_4. This results in two possible SV positions (SV_{top} and SV_{mid}) as depicted in Fig. 2A. Both SV_{top} and SV_{mid} models were constructed and tested for molecular H_2O_2 adsorption via two widely accepted adsorption configurations: end-on versus side-on (Fig. 2A). It was found that H_2O_2 adsorption was thermodynamically favorable on Fe_3S_4 (011) surfaces, even in the absence of SVs, with a large exothermal behavior and adsorption energies as high as −5.77 eV (O—O bond length: 1.525 Å) and −7.15 eV (O—O bond length: 1.526 Å) for end-on adsorption and side-on adsorption, respectively. The presence of SVs on Fe_3S_4 (011) surfaces appreciably increased the adsorption energies to −9.8 eV (SV_{top}) and −10.42 eV (SV_{mid}) via end-on adsorption. Importantly, the molecular H_2O_2 spontaneously dissociated to two •OH at SV_{mid} sites (O—O bond length: 2.501 Å) and was effectively activated at SV_{top} sites for dissociation (O—O bond length: 1.541 Å). This provides theoretical evidence for SV-dependent H_2O_2 activation because the SV-free surface only slightly activated the O—O bond length of adsorbed H_2O_2 from 1.515 Å (free H_2O_2) to 1.525 Å (end-on adsorption) or 1.526 Å (side-on adsorption; Fig. 2B—C). SV-promoted H_2O_2 dissociation was also observed for side-on H_2O_2 adsorption on the Fe_3S_4 (011) surface, with adsorbed •OH spontaneously generated after H_2O_2 approached SV_{top} (O—O bond length: 4.491 Å) or SV_{mid} (O—O bond length: 3.151 Å) sites (Fig. 2C). Notably, the adsorption energy of H_2O_2 on SV_{mid} sites (−6.01 eV) was reduced compared to its interactions with SV-free Fe_3S_4 (011) surfaces (−7.15 eV). Based on these theoretical calculations, we posit that H_2O_2 preferentially adsorbs at SVs of Fe_3S_4 (011) where it

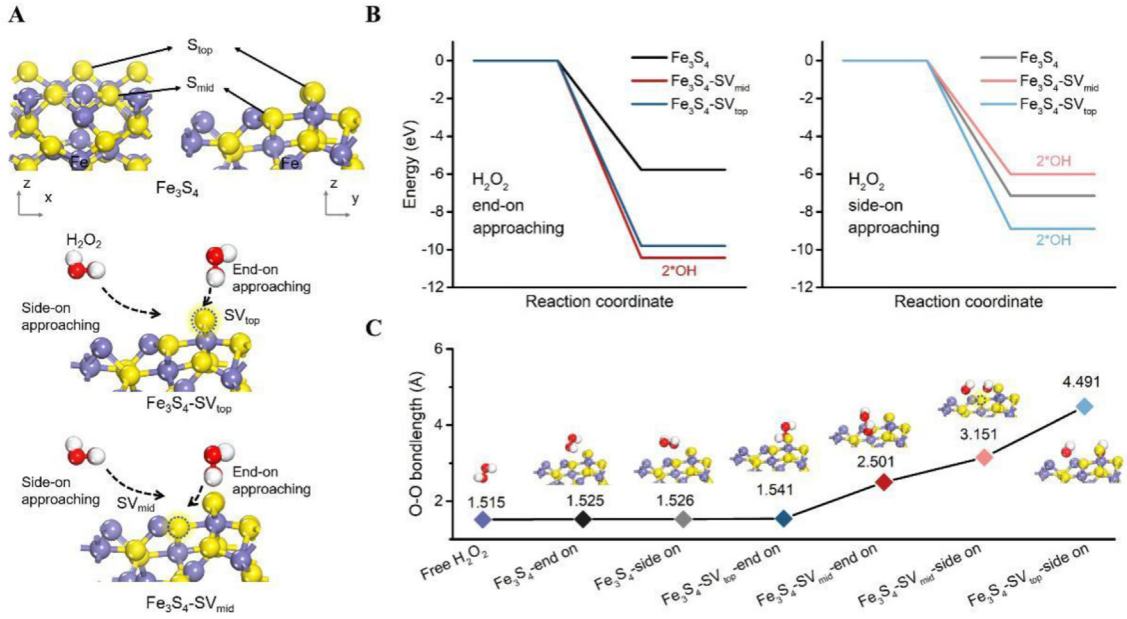

Fig. 2. (A) Schematic atomic configurations of idealized Fe_3S_4 (011) facet and corresponding counterparts of SV Fe_3S_4. (B) Energy diagrams of H_2O_2 adsorption on Fe_3S_4-011-SV via end-on approaching and side-on approaching. (C) O–O bond length of H_2O_2 plotted against different adsorption configurations.

is subsequently decomposed to •OH.

3.3. Peroxidase-like activity of Fe_3S_4 with varying SVs

To investigate peroxidase-like activity of SVs in Fe_3S_4, TMB was selected as a colorimetric indicator to detect the decomposition of H_2O_2. TMB oxidizes to TMB_{ox} upon reaction with H_2O_2/Fe_3S_4 and forms a bright blue suspension (Fig. 3A - inset). The UV–vis absorption spectra displayed a specific absorption peak at 652 nm. The absorbance intensity of FS-100 (1.64 a.u.) was much higher than that of FS-0 (0.28 a.u.), confirming the important role of SVs on peroxidase-like activity of Fe_3S_4.

As the peroxidase-like activity of nanozymes is extremely dependent on experimental conditions, we systematically investigated the effects of solution temperature, pH and Fe_3S_4 dosage on peroxidase-like activity of SV-rich Fe_3S_4 (FS-100). With respect to temperature, absorbance (652 nm) in the FS-100/H_2O_2/TMB system gradually increased from 1.32 to 1.64 and subsequently decreased to 1.41 as the temperature increased from 10 to 40 °C and 60 °C, respectively (Fig. 3B). Maximum peroxidase-like activity at 40 °C was consistent with a previous study [38]. Absorbance (652 nm) sharply increased to ~1.55 with increasing solution pH from 2.0 to 3.0–4.0, and then abruptly decreased to 0.05 with a further pH increase to 5.0 (Fig. 3C). Consequently, the highest activity was observed at pH 4.0, possibly ascribing to efficient Fenton-like activity of FS-100 in the pH range of 3.0–4.0 [39]. Absorbance (652 nm) gradually increased to 1.63 as the dosage of FS-100 increased to 30 μg/mL, and then remained stable with further dosage increases from 30 to 80 mg/L (Fig. 3D). These trials provided the following optimized experimental conditions: solution temperature = 40 °C, initial solution pH = 4.0; and nanozyme dosage (Fe_3S_4) = 30 μg/mL.

To confirm SV-dependent peroxidase-like activities of Fe_3S_4, steady-state kinetics for FS-100, FS-50, FS-25 and FS-0 were investigated using variable TMB and H_2O_2 concentrations under the optimized experimental conditions. Michaelis-Menten model curves are plotted in Fig. S6 for SV-based Fe_3S_4 in TMB and H_2O_2 concentration ranges of 0.1–1.6 mM and 0.01–0.8 mM, respectively. The Michaelis-Menten constant (K_m) and maximum reaction velocity (V_{max}) were calculated from Lineweaver-Burk plots (Fig. S6 - inset and Table 1). The K_m values for FS-100, FS-50, FS-25 and FS-0 with TMB were 0.161, 0.201, 0.670, and 0.175 mM, respectively. As lower K_m values indicate a stronger affinity of enzymes for a substrate, we conclude that SV-rich Fe_3S_4 has a relatively stronger affinity for TMB than SV-poor Fe_3S_4. The K_m (TMB) of the FS-100 (0.161 mM) was much lower than reported values for HRP (0.434 mM), GO-Fe_3S_4 (0.19 mM), and $ZnFe_2O_4$ (0.85 mM) (Table S3), suggesting a relatively high affinity of FS-100 for TMB. In addition, the calculated K_m (0.111 mM) for SV-rich Fe_3S_4 with H_2O_2 as a substrate was lower than that of the SV-poor Fe_3S_4, HRP and other nanozymes, confirming the stronger affinity of SV-rich Fe_3S_4 toward H_2O_2 than those of natural enzymes and other mimics. In sum, these results confirm that the surface defects of the SV-rich Fe_3S_4 nanozyme accelerate the diffusion of analytes and enhance enzymatic activity.

3.4. Mechanism for enhanced peroxidase-like activity of SV-rich Fe_3S_4

The theoretical calculations suggested that SV-based Fe_3S_4 promotes H_2O_2 dissociation to generate •OH. To verify these findings, TA was used as a probe to quantitatively determine •OH generation by Fe_3S_4 with varying SVs. Concentrations of •OH increased with increasing reaction time indicating a continuous decomposition of H_2O_2 catalyzed by Fe_3S_4 (Fig. 4A). The maximum •OH concentration with FS-100 was much higher than those of FS-50, FS-25 and FS-0. The •OH generation process followed a zero-order kinetic model, and the •OH generation constant for FS-100 (5.38×10^{-2} μM/min) was 7 times that of FS-0 (7.7×10^{-3} μM/min). Due to potential surface area effects on catalyst reactivity, the •OH generation constants for Fe3S4 were normalized with specific surface area (Table S2). Notably, the surface area normalized •OH generation constant for FS-100 was more than 6 times that of FS-0, ruling out surface area effects as the primary driver of the differences in •OH generation constants. Thus, we conclude that the SVs on Fe_3S_4 nanosheets promote •OH generation.

Dissolved ferrous ions released from the dissolution of Fe_3S_4 may also contribute to the decomposition of H_2O_2 to generated

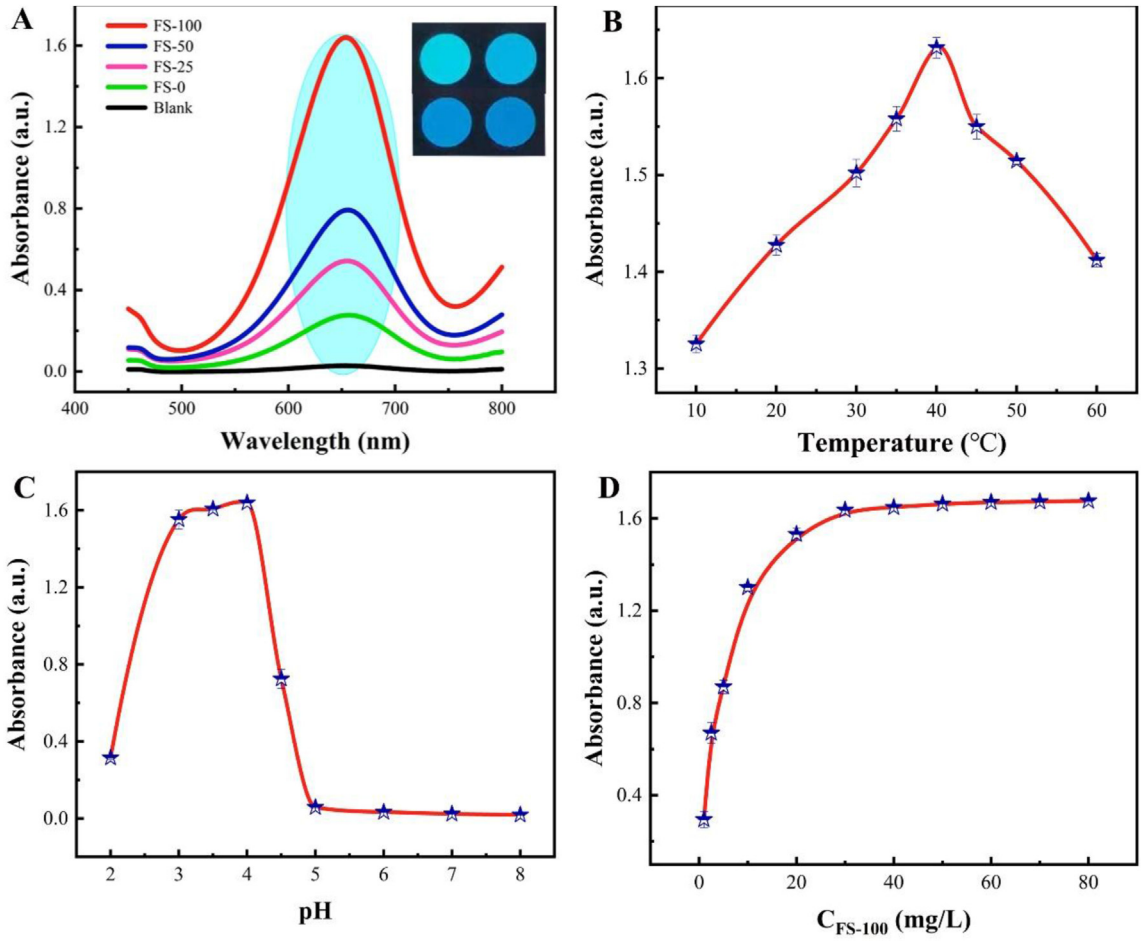

Fig. 3. (A) UV–Vis spectra of the reaction solution in the presence and absence of Fe_3S_4. The concentration of TMB, H_2O_2 and Fe_3S_4 were 6 mM, 30 mM and 30 μg/mL, respectively. The effects of reaction conditions on the peroxidase-like activity of FS-100: (B) temperature; (C) pH; (D) FS-100 concentration.

Table 1
Kinetic parameters for as-synthesized FS-0, FS-25, FS-50 and FS-100 nanosheets.

Catalyst	Substrate	K_m (mM)	V_{max} (10^8 M/s)
FS-100	H_2O_2	0.111	13.12
	TMB	0.161	14.71
FS-50	H_2O_2	0.505	7.89
	TMB	0.201	11.33
FS-25	H_2O_2	0.814	5.98
	TMB	0.670	8.77
FS-0	H_2O_2	1.006	5.69
	TMB	0.175	5.88

•OH. To examine this mechanism, we measured dissolved Fe(II) concentrations in the SV-based Fe_3S_4/NaAc buffer system without H_2O_2 addition. Dissolved Fe(II) concentrations were (μg/mL): 0.12 (FS-0), 0.14 (FS-25), 0.18 (FS-50) and 3.21 (FS-100) (Fig. 4B). We then added equal concentrations of Fe(II) to NaAc buffers in the presence of H_2O_2. Concentrations of •OH generated from Fe(II) additions were much lower than those corresponding to SV-based Fe_3S_4 assays. Addition of 14.0 μg/mL Fe(II), calculated as the complete dissolution of Fe_3S_4, resulted in production of only 0.215 μM•OH, suggesting a limited contribution of Fenton/Fenton-like reactions mediated by Fe(II)/Fe(III) dynamics from Fe_3S_4 (Fig. 4C). Thus, we attribute the higher •OH generation constant for FS-100 to higher SV concentrations on Fe_3S_4, which is in general agreement with the theoretical calculations.

3.5. Colorimetric detection of glucose with SV-rich Fe_3S_4

Benefiting from H_2O_2-enhanced dissociation capacity for •OH generation, SV-rich Fe_3S_4 (FS-100) was identified as an efficient nanozyme for selective detection of glucose in GOD-catalyzed methods. To test the efficacy of SV-rich Fe_3S_4 nanozyme assays for glucose quantification, we examined detection of glucose across a range of concentrations using FS-100, GOD, and TMB in a NaAc buffer solution (20 mM, pH = 4.0). The 652-nm absorbance increased linearly with increasing glucose concentrations in the range of 0.5–150 μM with a limit of detection (LOD) as low as 0.1 μM (Fig. S7). The analytical performance of the GOD-catalyzed methods based on SV-rich Fe_3S_4 (FS-100) is also compared with other previously reported nanozymes for detection of glucose. As summarized in Table S4, the LOD of SV-rich Fe_3S_4 (FS-100) (0.1 μmol/L) is lower than those of Fe_3O_4 (30 μM) [10], $CoFe_2O_4$ (0.15 μM) [18], $ZnFe_2O_4$ (0.30 μM) [38], Fe_3O_4/MoS_2 (2.40 μM) [40], Fe_3O_4/GO (0.74 μM) [41], and PB/MIL-101(Fe) (0.15 μM) [42], respectively. Moreover, the linear range of this assay based on SV-rich Fe_3S_4 (FS-100) (0.50–100 μM) is better than those of $CoFe_2O_4$ (2.40–100 μM) [18], $ZnFe_2O_4$ (1.25–18.75 μM) [38], and PB/MIL-101(Fe) (2.40–100 μM) [42], but is narrower than those of Fe_3O_4 (50–1000 μM) [10], Fe_3O_4/MoS_2 (5–150 μM) [40] and, Fe_3O_4/GO (2–200 μM) [41].

To test for selectivity and matrix interferences of the peroxidase-like activity in SV-rich Fe_3S_4 for glucose detection, relatively high concentrations (2.5 mM) of carbohydrates, such as maltose, lactose, fructose and L-glucose, were selected as potential

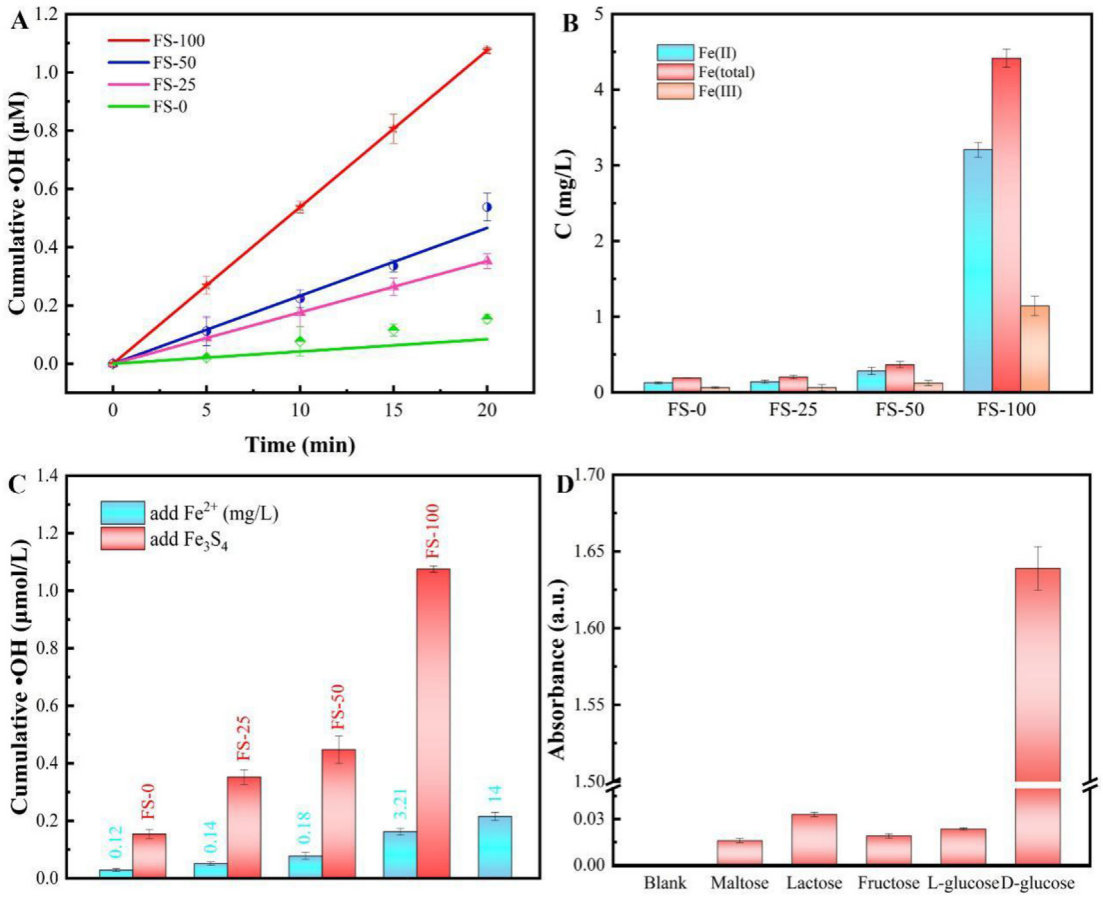

Fig. 4. (A) Generation rate of •OH in the presence of Fe_3S_4 nanosheets. (B) The concentration of dissolved Fe^{2+} in the Fe_3S_4/NaAc buffer system. (C) Comparison of the amount of •OH generated when Fe^{2+} and Fe_3S_4 nanosheets were added. (D) Selectivity of colorimetric method for glucose detection (carbohydrate concentrations: 0.5 mM glucose, 2.5 mM maltose, 2.5 mM fructose, 2.5 mM lactose). Error bars represent the standard deviation of three measurements.

interfering compounds. Background absorbance values were lower than 0.05 in the presence of maltose, lactose, fructose and L-glucose, indicating that specificity/interference issues had minimal effects on the SV-rich Fe_3S_4 system for glucose detection (Fig. 4D).

Finally, the feasibility of the proposed method for detecting glucose concentrations in human serum samples was tested on human blood samples using the optimized method. Table S5 summarizes the detection results by the newly developed colorimetric method using SV-rich Fe_3S_4 with peroxidase-like activity. Detected glucose concentrations ranged from 3.0 to 11.0 mM in the ten human serum samples. Compared to standard assay kits for glucose detection, the SV-rich Fe_3S_4 nanozyme assay produced relative recoveries of 93.7–101.4% with a relative error <7%. These results confirm that the newly developed method based on the SV-rich Fe_3S_4 nanozyme meets the strict requirements for glucose detection in human serum.

3.6. Smartphone application for glucose detection

Following optimization and validation of the SV-rich Fe_3S_4-catalyzed assay for glucose detection, we developed a smartphone application to determine glucose concentration in human serum samples by quantifying the intensity of the colorimetric reaction. Data analysis was performed by an automated smartphone App, and the analytical result displayed on the phone screen. As shown for a representative image (Scheme 2H), color intensity (~652 nm) increases with increasing glucose concentrations. Pixel intensities of the pit regions were plotted *versus* glucose concentrations to develop a standard curve. The linear range (LR) between pixel intensities and glucose concentrations was 5–100 μM and yielded a regression equation of $y = 187.362 + 0.024x\text{-}0.004x^2$ ($R^2 = 0.994$), where y is pixel intensity and x is the reciprocal of glucose concentration. The limit of detection (LOD) for glucose was 1.5 μM at a S/N = 3. After subjecting a serum sample to enzymatic reaction, glucose is automatically detected by the smartphone "Thing Identify" software application. Compared to detection results by standard assay kits, the relative recoveries for glucose in human serum samples ranged from 94.4 to 107.9% with a relative standard deviation for three replicates in the range of 1.2–5.8% (Table S5). These excellent metrics indicate that the newly developed method is convenient, cheap, quick and accurate for point-of-care diagnosis.

4. Conclusions

A series of SV-rich and -poor magnetic Fe_3S_4 nanosheets was prepared by changing the EG: H_2O ratio in the solvothermal process. The resulting Fe_3S_4 nanosheets were employed to detect serum glucose concentrations using a colorimetric assay. SV concentrations increased with increasing EG: H_2O ratios. The peroxidase-like activity of SV-rich Fe_3S_4 (FS-100) was significantly higher than that of SV-poor Fe_3S_4 (FS-0), which was ascribed to greater efficiency of SVs in Fe_3S_4 nanosheets to adsorb and decompose H_2O_2 to •OH. The catalytic kinetics of FS-100 nanozymes for electron transfer between TMB and H_2O_2 followed typical

Michaelis-Menten dynamics. Using the newly developed Fe_3S_4 nanozyme assay, glucose concentrations in human serum were detected with a LR of 0.5–150 μM and a LOD of 0.1 μM (S/N = 3). A smartphone App (Thing Identify) was designed and applied for efficient and accurate detection of serum glucose in humans. This study demonstrates the important role of surface defects in nanozymes for generating peroxidase-like activity. The newly developed SV-rich Fe_3S_4-catalytic colorimetric reaction was combined with a smartphone App to provide rapid, cheap, convenient and accurate glucose detection for point-of-care diagnosis.

CRediT authorship contribution statement

Wei Liu: Data curation. **Jinrong Tian:** Writing - original draft, Software, Methodology. **Chengliang Mao:** Software. **Zhenfeng Wang:** Software. **Jia Liu:** Methodology. **Randy A. Dahlgren:** Writing - review & editing. **Lizhi Zhang:** Investigation. **Xuedong Wang:** Conceptualization, Project administration, Supervision.

Declaration of competing interest

The authors declare that they have no known competing financial interests or personal relationships that could have appeared to influence the work reported in this paper.

Acknowledgements

We acknowledge the financial support from the National Science Foundation of China (Grants 21707105 and 21876125), Natural Science Foundation of Zhejiang Province (LY19B070010), Zhejiang Province Public Welfare Technology Application Research Project (LGF19B070008 and LGF19B070009), and Research and Development Fund of Wenzhou Medical University (Grant QTJ16013).

Appendix A. Supplementary data

Supplementary data to this article can be found online at https://doi.org/10.1016/j.aca.2020.06.056.

References

[1] Standards of medical care in diabetes-2017 A bridged for primary care providers, Clin. Diabetes 35 (2017) 5–26.
[2] C.J. Chen, W.L. Liao, C.T. Chang, Y.N. Lin, F.J. Tsai, Identification of urinary metabolite biomarkers of Type 2 diabetes nephropathy using an untargeted metabolomic approach, J. Proteome Res. 17 (2018) 3997–4007.
[3] N.H. Cho, J.E. Shaw, S. Karuranga, Y. Huang, J.D. Rocha Fernandes, A.W. Ohlrogge, B. Malanda, IDF diabetes atlas: global estimates of diabetes prevalence for 2017 and projections for 2045, Diabetes Res. Clin. Pract. 138 (2018) 271–281.
[4] P. Hsiao, C. Chen, Insights for realizing ultrasensitive colorimetric detection of glucose based on carbon/silver core/shell nanodots, ACS Appl. Bio. Mater. 2 (2019) 2528–2538.
[5] S.S. Jiang, Y.F. Zhang, Y.C. Yang, Y. Huang, G.C. Ma, Y.X. Luo, P. Huang, J. Lin, Glucose oxidase-instructed fluorescence amplification strategy for intracellular glucose detection, ACS Appl. Mater. Interfaces 11 (2019) 10554–10558.
[6] Y. Duan, Y.J. Huang, S.Y. Chen, W.Y. Zuo, B.F. Shi, Cu-doped carbon dots as catalysts for the chemiluminescence detection of glucose, ACS Omega 4 (2019) 9911–9917.
[7] Y.X. Zhang, J.Y. Xu, J.F. Xia, F.F. Zhang, Z.H. Wang, MOF-derived porous Ni_2P/Graphene composites with enhanced electrochemical properties for sensitive nonenzymatic glucose sensing, ACS Appl. Mater. Interfaces 10 (2018) 39151–39160.
[8] C. Lu, X.J. Liu, Y.F. Li, F. Yu, L.H. Tang, Y.J. Hu, Y.B. Ying, Multifunctional janus hematite–silica nanoparticles: mimicking peroxidase-like activity and sensitive colorimetric detection of glucose, ACS Appl. Mater. Interfaces 7 (2015) 15395–15402.
[9] R. Breslow, Biomimetic chemistry and artificial enzymes: catalysis by design, Acc. Chem. Res. 28 (1995) 146–153.
[10] H. Wei, E. Wang, Fe_3O_4 magnetic nanoparticles as peroxidase mimetics and their applications in H_2O_2 and glucose detection, Anal. Chem. 80 (2008) 2250–2254.
[11] L.Z. Gao, J. Zhuang, L. Nie, J.B. Zhang, Y. Zhang, N. Gu, T.H. Wang, J. Feng, D.L. Yang, S. Perrett, X.Y. Yan, Intrinsic peroxidase-like activity of ferromagnetic nanoparticles, Nat. Nanotechnol. 2 (2007) 577–583.
[12] J. Liu, L.J. Meng, Z.F. Fei, P.J. Dyson, X.N. Jing, X. Liu, MnO_2 nanosheets as an artificial enzyme to mimic oxidase for rapid and sensitive detection of glutathione, Biosens. Bioelectron. 90 (2017) 69–74.
[13] P.F. Zhan, Z.G. Wang, N. Li, B.Q. Ding, Engineering gold nanoparticles with DNA ligands for selective catalytic oxidation of chiral substrates, ACS Catal. 5 (2015) 1489–1498.
[14] L. Han, C. Li, T. Zhang, Q. Lang, A. Liu, Au@Ag heterogeneous nanorods as nanozyme interfaces with peroxidase-like activity and their application for one-pot analysis of glucose at nearly neutral pH, ACS Appl. Mater. Interfaces 26 (2015) 14463–14470.
[15] Y.K. Xia, M.M. Liu, L.L. Wang, A. Yan, W.H. He, M. Chen, J.M. Lan, J.X. Xu, L.H. Guan, J.H. Chen, A visible and colorimetric aptasensor based on DNA-capped single-walled carbon nanotubes for detection of exosomes, Biosens. Bioelectron. 92 (2017) 8–15.
[16] Y.J. Song, X.H. Wang, C. Zhao, K.G. Qu, J.S. Ren, X.G. Qu, Label-free colorimetric detection of single nucleotide polymorphism by using single-walled carbon nanotube intrinsic peroxidase-like activity, Chem. Eur J. 16 (2010) 3617–3621.
[17] T.M. Chen, X.J. Wu, J.X. Wang, G.W. Yang, WSe_2 few layers with enzyme mimic activity for high-sensitive and high-selective visual detection of glucose, Nanoscale 9 (2017) 11806–11813.
[18] W.B. Shi, X.D. Zhang, S.H. He, Y.M. Huang, $CoFe_2O_4$ magnetic nanoparticles as a peroxidase mimic mediated chemiluminescence for hydrogen peroxide and glucose, Chem. Commun. 47 (2011) 10785–10787.
[19] G. Vinothkumar, A.I. Lalitha, K.S. Babu, Cerium phosphate-cerium oxide heterogeneous composite nanozymes with enhanced peroxidase-like biomimetic activity for glucose and hydrogen peroxide sensing, Inorg. Chem. 58 (2019) 349–358.
[20] M.K. Masud, S. Yadav, M.N. Islam, N. Nguyen, C. Salomon, R. Kline, H. Alamri, Z.A. Alothman, Y. Yamauchi, M. Hossain, M. Shiddiky, Gold-loaded nanoporous ferric oxide nanocubes with peroxidase-mimicking activity for electrocatalytic and colorimetric detection of autoantibody, Anal. Chem. 89 (2017) 11005–11013.
[21] X.Q. An, Q.W. Tang, H.C. Lan, H.J. Liu, J.H. Qu, Polyoxometalates/TiO_2 Fenton-like photocatalysts with rearranged oxygen vacancies for enhanced synergetic degradation, Appl. Catal., B 244 (2019) 407–413.
[22] H. Li, J. Shang, Z.P. Yang, W.J. Shen, Z.H. Ai, L.Z. Zhang, Oxygen vacancy associated surface Fenton chemistry: surface structure dependent hydroxyl radicals generation and substrate dependent reactivity, Environ. Sci. Technol. 51 (2017) 5685–5694.
[23] J.Z. Liao, L.C. Chen, M.L. Sun, B. Lei, X.L. Zeng, Y.J. Sun, F. Dong, Improving visible-light-driven photocatalytic NO oxidation over BiOBr nanoplates through tunable oxygen vacancies, Chin. J. Catal. 39 (2018) 779–789.
[24] X.S. Sun, X. Luo, X.D. Zhang, J.F. Xie, S. Jin, H. Wang, X.S. Zheng, X.J. Wu, Y. Xie, Enhanced superoxide generation on defective surfaces for selective photooxidation, J. Am. Chem. Soc. 141 (2019) 3797–3801.
[25] S. Tongay, J. Zhou, C. Ataca, J. Liu, J.S. Kang, T.S. Matthews, L. You, J. Li, J.C. Grossman, J.Q. Wu, Broad-range modulation of light emission in two-dimensional semiconductors by molecular physisorption gating, Nano Lett. 13 (2013) 2831–2836.
[26] H.Y. Nan, Z.L. Wang, W.H. Wang, Z. Liang, Y. Lu, Q. Chen, D.W. He, P.P. Tan, F. Miao, X.R. Wang, Strong photoluminescence enhancement of MoS_2 through defect engineering and oxygen bonding, ACS Nano 8 (2014) 5738–5745.
[27] M.Y. Xing, W.J. Xu, C.C. Dong, Y.C. Bai, J.B. Zeng, Y. Zhou, J.L. Zhang, Y.D. Yin, Metal sulfides as excellent co-catalysts for H_2O_2 decomposition in advanced oxidation processes, Inside Chem. 4 (2018) 1359–1372.
[28] C.P. Ding, Y.H. Yan, D.S. Xiang, C.L. Zhang, Y.Z. Xian, Magnetic Fe_3S_4 nanoparticles with peroxidase-like activity, and their use in a photometric enzymatic glucose assay, Microchim Acta 183 (2015) 625–631.
[29] W. Liu, L.D. Jin, J. Xu, J. Liu, Y.Y. Li, P.P. Zhou, C.C. Wang, Insight into pH dependent Cr(VI) removal with magnetic Fe_3S_4, Chem. Eng. J. 359 (2019) 564–571.
[30] W. Liu, Z.H. Ai, R.A. Dahlgren, L.Z. Zhang, X.D. Wang, Adsorption and reduction of roxarsone on magnetic greigite (Fe_3S_4): indispensable role of structural sulfide, Chem. Eng. J. 330 (2017) 1232–1239.
[31] Y.Y. Li, J. Hu, W. Liu, L.D. Jin, P.P. Zhou, Y.X. Zhang, B. Zhang, R.A. Dahlgren, X.D. Wang, Y.K. Zhou, Magnetic effervescent tablet-assisted ionic liquid based dispersive liquid-liquid microextraction of polybrominated diphenyl ethers in liquid matrix samples, Talanta 195 (2018) 785–795.
[32] X.D. Wang, J. Xu, J. Liu, F. Xia, C.C. Wang, R.A. Dahlgren, W. Liu, Mechanism of Cr(VI) removal by magnetic greigite/biochar composites, Sci. Total Environ. 700 (2020) 134414.
[33] S. Shit, W. Jang, S. Bolar, N. Murmu, H. Koo, T. Kuila, Effect of the solvent ratio (ethylene glycol/water) on the preparation of an iron sulfide electrocatalyst and its activity towards overall water splitting, Chem. Electro. Chem. 6 (2019) 3199–3208.
[34] W. Liu, Y.Y. Wang, Z.H. Ai, L.Z. Zhang, Hydrothermal synthesis of FeS_2 as a high-efficiency Fenton reagent to degrade alachlor via superoxide-mediated Fe(II)/Fe(III) cycle, ACS Appl. Mater. Interfaces 7 (2015) 28534–28544.
[35] H. Li, L.Z. Zhang, Oxygen vacancy induced selective silver deposition on the {001} facets of BiOCl single-crystalline nanosheets for enhanced Cr(VI) and sodium pentachlorophenate removal under visible light, Nanoscale 6 (2014)

7805–7810.
[36] Y.X. Zhou, Y.T. Zhao, X.G. Wu, W.Q. Yin, J.H. Hou, S.S. Wang, K. Feng, X.Z. Wang, Adsorption and reduction of hexavalent chromium on magnetic greigite (Fe_3S_4)-CTAB: leading role of Fe(II) and S(-II), RSC Adv. 8 (2018) 31568–31574.
[37] A.A. Rownaghi, T.Y. Hin, T.W. Jiunn, Influence of the ethylene glycol, water treatment and microwave irradiation on the characteristics and performance of VPO catalysts for n-butane oxidation to maleic anhydride, Catal. Lett. 130 (2009) 593–603.
[38] L. Su, J. Feng, X.M. Zhou, C.L. Ren, H.H. Li, X.G. Chen, Colorimetric detection of urine glucose based $ZnFe_2O_4$ magnetic nanoparticles, Anal. Chem. 84 (2012) 5753–5758.
[39] L.H. Jin, Z. Meng, Y.Q. Zhang, S.J. Cai, Z.H. Zhang, C. Li, L. Shang, Y.H. Shen, Ultrasmall Pt nanoclusters as robust peroxidase mimics for colorimetric detection of glucose in human serum, ACS Appl. Mater. Interfaces 9 (2017) 10027–10033.
[40] V. Nandwana, W.Y. Huang, Y. Li, Y.P. Dravid, One-pot green synthesis of Fe_3O_4/MoS_2 0D/2D nanocomposites and their application in noninvasive point-of-care glucose diagnostics, ACS Appl. Nano Mater. 1 (2018) 1949–1958.
[41] Y.L. Dong, H.G. Zhang, Z. Rahman, L. Su, X.J. Chen, X.G. Chen, Graphene oxide-Fe_3O_4 magnetic nanocomposites with peroxidase-like activity for colorimetric detection of glucose, Nanoscale 4 (2012) 3969–3976.
[42] F.J. Cui, Q.F. Deng, L. Sun, Prussian blue modified metal–organic framework MIL-101(Fe) with intrinsic peroxidase-like catalytic activity as a colorimetric biosensing platform, RSC Adv. 5 (2015) 98215–98221.